JCTC Journal of Chemical Theory and Computation

Article

pubs.acs.org/JCTC

Solution Properties of Hemicellulose Polysaccharides with Four Common Carbohydrate Force Fields

Jörg Sauter and Andrea Grafmüller*

Theory and Bio-Systems, Max Planck Institute of Colloids and Interfaces, Potsdam, Germany

ABSTRACT: Hemicellulose polysaccharides play an important role in the swelling behavior of the primary plant cell wall, and molecular dynamics simulations provide the means of gaining a concise understanding of the interactions of hemicellulose polysaccharides with water. Here, we compare four of the main polysaccharide force fields (CHARMM36 TIP3P, GROMOS56A6$_{CARBO}$ SPC, GLYCAM06h TIP3P, and GLYCAM06h TIP5P) for the most abundant hemicellulose backbone components. In particular, we compare aggregation, diffusion coefficients, system density, and investigate the free energy of hydration of saccharides in water. We find that the saccharides show nonphysical aggregation at low concentrations with the GLYCAM06h TIP3P force field, which can be rectified by the use of the TIP5P water model. As a result of the aggregation, GLYCAM06h TIP3P does not lead to reasonable diffusion coefficients whereas the diffusion coefficients, as well as the system density, agrees best with experimental data for the GLYCAM06h TIP5P force field. Overall, GLYCAM06h TIP5P gives good agreement with experimental free energy of hydration data for small saccharides. In addition, the free energy of hydration for short polysaccharides calculated with the GLYCAM06h TIP5P force field is consistent with the radial distribution functions between the polysaccharides and water, the hydration number of the polysaccharides, and the hydrogen bonds formed in the system.

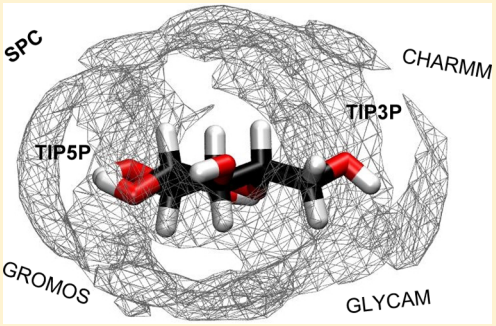

1. INTRODUCTION

The primary plant cell wall consists of crystalline cellulose microfibrils embedded into an amorphous matrix of hemicellulose and pectin in highly varying concentrations, depending on the plant species[1] and cell type. It is highly stress resistant while it is, at the same time, sensitive to hydration and can significantly swell, as a function of water content.[2,3] This swelling can be direction-dependent, because of the angle at which the cellulose microfibrils are embedded into the matrix polysaccharides.[4] Such direction-dependent swelling plays an important role in stress generation in tension wood,[5] the opening of ice plant seed capsules[6] or pine cones,[7] and many other examples. In addition, the primary cell wall polysaccharides store a significant amount of energy. However, it has proven difficult to utilize this energy, because of the recalcitrance encountered when extracting polysaccharides into a usable form due to the complex architecture of the plant cell wall.[1] A molecular level understanding of the structure and dynamics of the plant cell wall constituents may help in the development of actuators or adaptive materials as well as new methods to overcome the plant cell wall recalcitrance.

Hemicellulose polysaccharides account for the main part of the polymer network into which the hygroscopically insensitive cellulose microfibrils are embedded. Therefore, the interactions of these polysaccharides with water are a key factor. Hemicelluloses are a class of branched polysaccharides. The most abundant types, xyloglucan, xylan, and mannan consist of a backbone of (1−4) linked β-D-glucose, β-D-xylose, and β-D-mannose[8] with short, species-dependent side-chains. The chemical structures of these monomers are shown in Figure 1a and a xyloglucan structure is shown in Figure 1b. Xyloglucans can reach a degree of polymerization (DP) up to

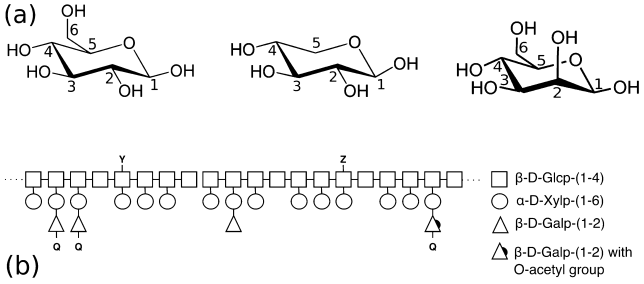

Figure 1. (a) Chemical structure of β-D-glucose, β-D-xylose, and β-D-mannose. (b) Structure of a xyloglucan. Position **Q**, **Y**, and **Z** can contain various substitutions.[11]

the order of 3500[9] and are generally shorter than cellulose, which can be found with a DP of up to 15 000.[10]

Molecular dynamics (MD) simulations have been successfully used for the simulation of biomolecules for many years. As the role of polysaccharides is recognized in an increasing number of biological systems, MD simulations of polysaccharides are gaining both importance and accuracy. Until now, most simulations of cell wall polysaccharides have been MD simulations of cellulose crystals. These studies have investigated the crystalline form of short cellulose[12−14] as well as the

Received: October 18, 2014
Published: March 11, 2015

DOI: 10.1021/ct500924f
J. Chem. Theory Comput. 2015, 11, 1765−1774

decrystallization process[15−18] and dissolution in ionic solutions.[19,20] In addition, the high-temperature behavior[21,22] has been studied.

On the other hand, the matrix polysaccharides have received very little attention. However, the conformational folding of the side chains of xyloglucan[23] and the interaction of xyloglucan and cellulose,[24−26] as well as xylan and cellulose interactions,[27] have been studied. In addition, the gelation of xyloglucan in ethanol/water mixtures has been investigated.[28]

MD simulations rely on the force field (FF) used and on the parametrization of the atomistic interactions. To maximize the predictive power, where little to no experimental data is available, systematic evaluations and comparisons are of significant importance to ensure that the FF correctly describes the system of interest. With respect to carbohydrate simulations, besides two recent general carbohydrate FF comparisons,[29,30] a recent article[31] has specifically compared the representation of the cellulose structure in different FFs with the main focus on the internal degrees of freedom. Significant differences between the investigated FFs were found underlining the importance of the FF choice.

Here, we compare the performance of different FFs for hemicellulose building blocks, with respect to the properties in solution and their specific interactions with water. We evaluate the aggregation, diffusion coefficients, and system density of β-D-glucose monomers at various concentrations in water, as well as the free energy of hydration for the small saccharides, where experimental results are available. The aggregation, diffusion, and density simulations are used for a comparison of the computational efficiency.

Free-energy methods have been successfully applied to obtain the free energy of hydration for many small molecules.[32−36] However, for larger molecules experimental data is unavailable, because of the low vapor pressures that must be measured precisely. In particular, for polysaccharides, the vapor pressure is hard to obtain experimentally. Therefore, we calculate the free energy of hydration for linear polysaccharides of the three main backbone monomers up to DP = 16, using the FF that showed best agreement with experimental data. In addition, we study the radial distribution functions (RDFs) between the polysaccharides and water and evaluate hydration numbers as well as hydrogen bonds. This analysis provides the means to further assess the reliability of the calculated free energy of hydration values.

2. METHODS

2.1. Molecular Dynamics Details and System Setup. We simulated the following four system types:

(i) multiple β-D-glucose monomers in water for the aggregation, diffusion, and density measurements at 298.15 K for comparison with experimental data using a quadratic box;
(ii) single α-D-xylose, α-D-glucose, and cellobiose (the chemical structure is shown in Figure 9a) molecules in water for the Gibbs free energy of hydration (ΔG) calculation and comparison to experimental data at 300 K using a dodecahedron box;
(iii) single solute molecules in water for the ΔG calculations for linear polysaccharides with DP up to 16 at 300 K using a dodecahedron box; in addition to the linear polysaccharides consisting of β-D-glucose, β-D-xylose, and β-D-mannose, we investigated a mixed polysaccharide consisting of alternating β-D-glucose and β-D-xylose; and
(iv) single solute molecules in water for the calculations of the radial distribution functions (RDFs), hydration numbers, and the hydrogen bond analysis for linear polysaccharides with DP at 300 K, using a dodecahedron box.

All computations were performed in GROMACS 4.6.4,[37] using periodic boundary conditions in the NPT ensemble. All covalent bonds involving hydrogen atoms were constrained with LINCS,[38] and all water models use Settle[39] constraints. Electrostatic interactions were treated with the Particle Mesh Ewald method,[40] using a 1.4 nm cutoff. A 1.4 nm cutoff was also used for the Lennard-Jones interactions. The pressure in the simulation was set to 1 bar with the Parinello−Rahmann barostat.[41,42]

Except for the free-energy calculations, we used the Leap-Frog integrator[43] with a 2 fs time-step size, and the temperature was controlled using the Nosé−Hoover thermostat.[44,45] For the free-energy calculations, we used Langevin Dynamics with the Stochastic Dynamics integrator[46] and a thermostat with a 1 fs time step size to obtain the correct ensemble for the single solute molecules in vacuum.

For CHARMM[47,48] and GROMOS,[49] the system was set up directly in GROMACS after the CHARMM parameters were converted to GROMACS. With CHARMM, the TIP3P[50] water model was used, whereas for GROMOS, we used the SPC water model.[51] The GLYCAM06h[52] topology and coordinate files were generated in Amber 12[53], using PDB files from the GLYCAM builder.[54] Afterward, they were converted to the GROMACS format using the glycam2gmx script,[55,56] followed by hydration in GROMACS with TIP3P or TIP5P[57] water. Energy minimization and equilibration were performed using standard protocols. For visualization, we used visual molecular dynamics (VMD).[58]

2.2. Aggregation and Diffusion. For the aggregation and diffusion calculations, we used from 29 up to 305 β-D-glucose monomers and from 6538 down to 4270 water molecules to create the respective concentrations between 0.25 mol kg^{-1} and 4 mol kg^{-1}. For all concentrations, the system consisted of 20 000 ± 331 atoms, not counting TIP5P lone pairs. The starting conformation was generated by multiplying the single solute system and the final NPT equilibration time was 200 ns. The data collection time was 200 ns and started after the equilibration.

To quantify aggregation, we used the RDF

$$g(r) = \frac{V}{N_p(N_p-1)}\left\langle \sum_i \sum_{i\neq j} \delta(r - |\mathbf{r}_i - \mathbf{r}_j|)\right\rangle \quad (1)$$

where $\mathbf{r}_i$ and $\mathbf{r}_j$ are the center of mass (COM) of β-D-glucose monomers i and j, respectively; N_p denotes the number of β-D-glucose monomers, V the volume, and $\langle\cdot\rangle$ the ensemble average.

The diffusion coefficient D was determined from the mean square displacement $m(t) = \langle|\mathbf{r}(t_0 + t) - \mathbf{r}(t_0)|^2\rangle_{t_0}$. Here, $\mathbf{r}(t)$ is the COM of a monomer at the time t and the mean $\langle\cdot\rangle_{t_0}$ is taken over both all monomers and all starting times 2 ns ≤ t_0 ≤ 25 ns. The diffusion cofficient is calculated by the Einstein relation[59]

$$D = \frac{\bar{m}}{6\delta} \quad (2)$$

DOI: 10.1021/ct500924f
J. Chem. Theory Comput. 2015, 11, 1765−1774

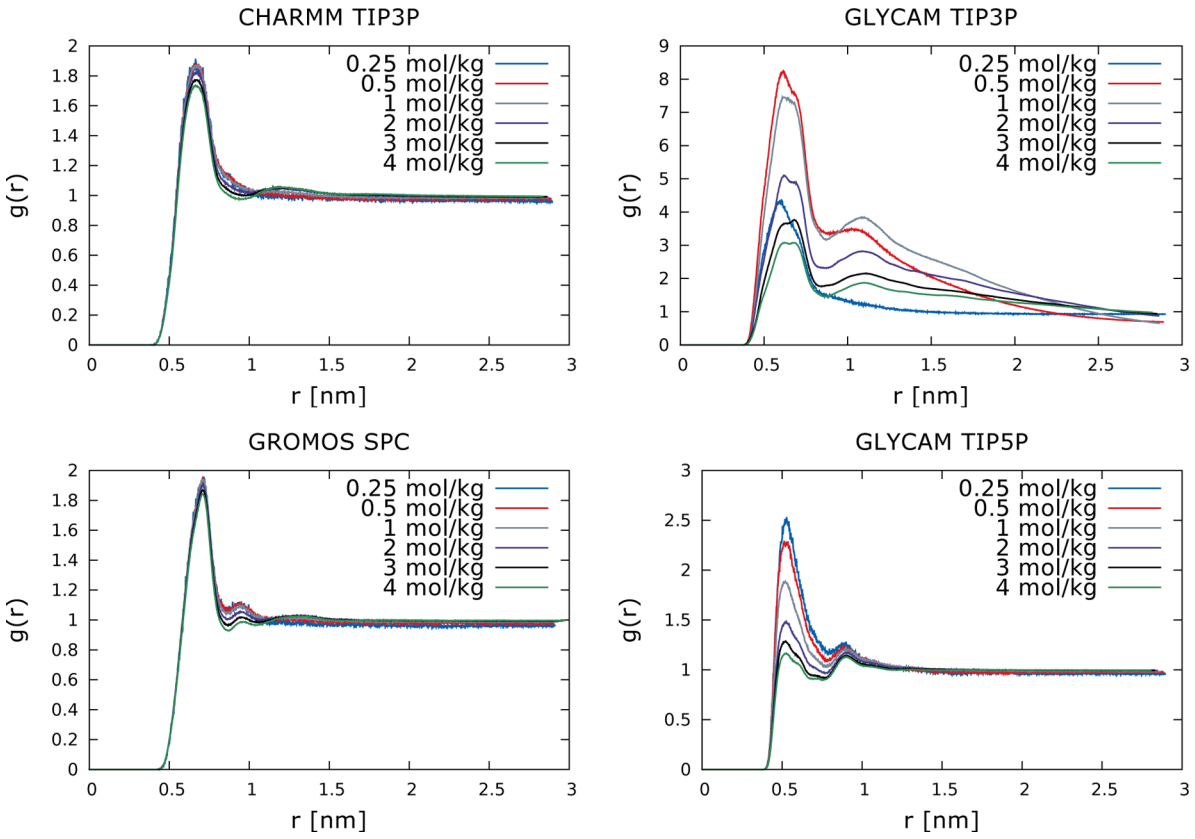

Figure 2. RDFs between β-D-glucose monomers (COM) in water for different concentrations and FFs. Note the different scales for the GLYCAM FFs.

with δ = 23 ns. The averaged mean square displacement $\bar{m}$ is obtained by a linear least-squares approximation of $m(t)$ for 2 ns $\leq t \leq$ 25 ns. An error estimate for the diffusion coefficient was obtained from the difference of the separately calculated $\bar{m}$ for $t \leq$ 12.5 ns and $t \geq$ 12.5 ns.

2.3. Free Energy of Hydration. The system was sampled for 5 ns and the first 500 ps were neglected as additional equilibration. The free energy output was written every 0.1 ps. We used the Bennett Acceptance Ratio[60,61] method to obtain ΔG, since it has proven accurate in previous comparisons.[62,63] To ensure overlap in phase space, the transition from the starting state to the end state was done by introducing 25 intermediate steps defined by the coupling parameter $\lambda \in [0,1]$. The total ΔG was calculated as the sum over all intermediate states. We insert the polysaccharide into the system as the phase space overlap, measured in terms of relative entropy,[64] is slightly better for insertion than removal of the saccharide.

The states with intermediate λ values were generated using the soft core potential U_{SC}^{λ}.[65,66] The attractive 6-term in the Lennard-Jones potential is shown in eq 3:

$$U_{SC}^{\lambda} = (1 - \lambda)U^0(r_0) + \lambda U^1(r_1) \quad (3)$$

where U^0 and U^1 denote the original 6-term of the Lennard-Jones potential at the decoupled and coupled state, respectively, and the radii are defined as $r_0 = (\alpha\sigma_0^6\lambda^p + r^6)^{(1/6)}$ and $r_1 = (\alpha\sigma_1^6(1 - \lambda)^p + r^6)^{1/6}$. The parameters α = 1 and p = 1 were used, and σ is determined by the Lennard-Jones parameters. The 12-term in the Lennard-Jones potential is defined analogously to eq 3.

The electrostatic interactions were switched on separately after the Lennard-Jones interactions and could therefore be coupled linearly. An error estimate was obtained by block averaging.

We evaluated the evolution of ΔG, as a function of simulation time, to ensure convergence. For the ΔG value of a β-D-glucose polymer with DP = 16, the method converges within the first 250 ps (750 ps total simulation time) and only minor changes in ΔG are observed afterward. Note that versions previous to GROMACS 4.6.4 are not able to handle the GLYCAM topology correctly, when performing free-energy calculations due to GROMACS Bug No.1315.

2.4. Polysaccharide Hydration. To obtain the RDF, hydration number, and hydrogen bonds of the linear polysaccharides with the GLYCAM TIP5P FF, we simulated the system for 400 ns. The RDF of water molecules (COM) around a monomer (COM) were calculated in analogy to eq 1. The hydration number is given by the number of water molecules within a distance of 0.36 nm to the polysaccharide measured by the minimal oxygen−oxygen distance. This distance is the first hydration shell for β-D-glucose, β-D-xylose, β-D-mannose given by the GLYCAM TIP5P FF. The criterion for hydrogen bonds was a maximal donor−acceptor distance of 0.35 nm and a hydrogen-donor−acceptor angle of <30°.

3. RESULTS AND DISCUSSION

3.1. Aggregation and Diffusion. Figure 2 compares the aggregation behavior of β-D-glucose monomers (COM) in water for the different FFs and concentrations. The RDFs for the CHARMM TIP3P and the GROMOS SPC FF show only a minor concentration dependence, with slightly increasing long-range correlations at r > 1 nm with increasing concentration. Simultaneously, the peak in the first coordination shell

DOI: 10.1021/ct500924f
J. Chem. Theory Comput. 2015, 11, 1765−1774

decreases slightly. For GROMOS SPC, this is also true for the second shell, while a second shell is not present at this distance for CHARMM TIP3P.

In contrast, the RDFs for both GLYCAM FFs show a strong variation with concentration. For GLYCAM TIP5P, the peak of the first coordination shell decreases more strongly than for either CHARMM TIP3P or the GROMOS SPC FF. The peak of the second coordination shell, which is present for GLYCAM TIP5P at the same distance as in the GROMOS SPC FF, also decreases slightly. For GLYCAM TIP3P, the peak for the first coordination shell at a concentration of 0.25 mol kg^{-1} is significantly higher than for any of the other FFs. With increasing concentration, starting from 0.5 mol kg^{-1}, the molecules begin to cluster, which is reflected in the very high first coordination shell and the appearance of a wide second peak, up to ∼2.5 nm, showing the presence of significant long-range correlations. Upon further increases in concentration, the magnitude of the peaks decreases again, as the saccharides take up more space of the simulation box; however, the long-range correlations remain present. In these simulations, most monomers bind to a single cluster of monomers within a few nanoseconds. Such aggregation is nonphysical at a concentration of 0.5 mol kg^{-1}, which is equivalent to roughly 90 g L^{-1}, whereas the solubility limit of β-D-glucose is 910 g L^{-1} at 298.15 K.[67]

To better understand the origin of the observed overaggregation in the GLYCAM TIP3P topology compared to CHARMM TIP3P, which uses the same water model, we analyze the influence of different contributions to the sugar−water interactions. The solubility of molecules in water is linked to their average polarity. Comparing the average dipole moments of β-D-glucose, we find a value of μ_{GLY} = 3.80 D at 0.25 mol kg^{-1} for GLYCAM, whereas for CHARMM and GROMOS, the average dipole moments are μ_{CH} = 4.07 D and μ_{GR} = 4.10 D, respectively. Thus, β-D-glucose molecules are less polar than with the CHARMM and GROMOS FFs, which will affect their solubility. On the other hand, we have a dipole moment of μ_{TIP3P} = 2.35 D for TIP3P water and μ_{TIP5P} = 2.29 D for TIP5P, so that the solubility consistently increases in the less polar water. However, the differences between the water models are relatively small, so that other effects are likely to play a role.

Nonetheless, if the saccharide charges in a GLYCAM TIP3P system are disabled, rendering the molecules completely unpolar, the aggregation becomes even stronger. Whereas, at a concentration of 0.5 mol kg^{-1}, the peak of the first coordination shell for the system with charges is $g(r) \approx 8$ (Figure 2), we have $g(r) \approx 22$ with disabled charges. A general conclusion, therefore, is that the aggregation is caused by the van der Waals interactions while the electrostatic interactions of the saccharides serve to reduce it, although insufficiently for GLYCAM TIP3P. Comparison of the FF parameters shows, that the most relevant difference in the Lennard-Jones parameters between CHARMM and GLYCAM is the significantly larger Lennard-Jones parameter ϵ for carbon. For CHARMM, ϵ = 0.133888 for all carbons except C6 (ϵ = 0.234304), while for GLYCAM, ϵ = 0.457730 for all carbons.

Related observations have been made by Hadden et al.[68] in the context of cellulose microfibril twist, for which the sugar−water interactions were shown to play a central role. It was found that replacing TIP3P by TIP5P water significantly reduces the twisting of cellulose microfibrils, and that microfibril twist is favored by van der Vaals interactions and counteracted by electrostatics.

Overall, the two studies show many parallels between factors promoting twist and aggregation. The solute−solvent hydrogen bond formation and directionality appears to be a determining factor for both phenomena. As shown in ref 68, it leads to a higher occupancy in the first hydration shell and a higher solute−solvent interaction energy. Here, a similar stronger affinity of TIP5P than TIP3P water to the saccharides is also found from the potential interaction energies. This increased solute−solvent affinity with TIP5P is found to be mainly due to the electrostatic interactions, as discussed in more detail in the context of hydration free energies in section 3.4.

Finally, the GLYCAM06-EP[69] FF, which introduces lone pairs on carbohydrate oxygen atoms enhances the effect of TIP5P on the microfibril twist.[68] Therefore, it might be expected to also affect the aggregation behavior. However, we found that use of the GLYCAM06-EP TIP5P FF has little additional effect on the systems, i.e., aggregation is observed starting from 0.5 mol kg^{-1} with GLYCAM06-EP TIP3P, whereas no aggregation appears with GLYCAM06-EP TIP5P. Thus, we can conclude that the improved structuring of the solute−solvent hydrogen bonds has a much more important effect on the aggregation behavior than the improvement of solute−solute hydrogen bonding introduced by GLYCAM06-EP.

Inversely to the overaggregation found for GLYCAM TIP3P, in simulations of high β-D-glucose concentrations of 7 mol kg^{-1}, i.e., roughly 1260 g L^{-1} (which is well above the solubility limit), no aggregation is observed for any FF except GLYCAM TIP3P. However, at this concentration, the system is below the glass-transition temperature,[70] so it is unclear whether the system equilibrates within 200 ns, especially since the aggregation for GLYCAM TIP3P also takes significantly longer than at lower concentrations. The question whether there is aggregation in supersaturated solutions for any other FF could be addressed by coarse-grained simulations, based on the respective FF, similar to the work reported by Molinero et al.[71]

In addition to the structural data, we compare the diffusion coefficients for the different FFs plotted in Figure 3, as a function of concentration. The results for all FFs deviate from the quasi-linear concentration dependence of the experimental data. For CHARMM TIP3P and GROMOS SPC, the calculated diffusion coefficients are higher than the exper-

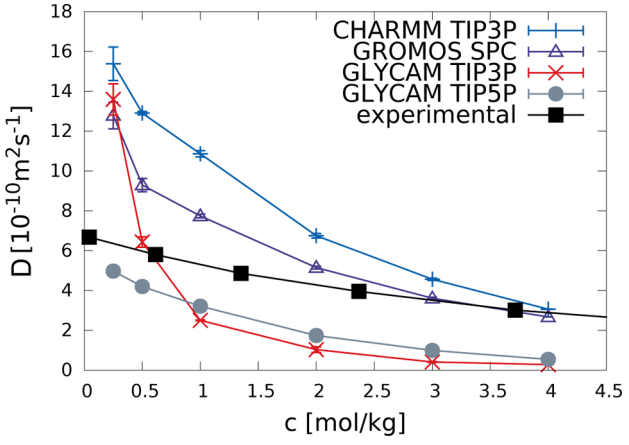

Figure 3. Diffusion D of β-D-glucose monomers in water at different concentrations c and FFs, in comparison to experimental data.[72]

DOI: 10.1021/ct500924f
J. Chem. Theory Comput. 2015, 11, 1765−1774

imental values at low concentrations. For CHARMM TIP3P, this has been discussed previously, and can partly be attributed to the nonphysically high TIP3P water self-diffusion.[73] The self-diffusion of TIP3P water[74] at 287.15 K is $D_{TIP3P} = 5.19 \times 10^{-10}$ m^2 s^{-1}, compared to an experimental value[75] of $D_{exp} = 2.30 \times 10^{-10}$ m^2 s^{-1}. For SPC water, the self-diffusion coefficient,[74] $D_{SPC} = 3.85 \times 10^{-10}$ m^2 s^{-1}, is closer to the experimental value, but still slightly too high. This is consistent with the diffusion coefficient of the saccharide system, which is a slight overestimate. For TIP5P water, the diffusion coefficient $D_{TIP5P} = 2.62 \times 10^{-10}$ m^2 s^{-1} is closest to the experimental value[74] and GLYCAM TIP5P best describes the diffusion of the saccharides, but somewhat underestimates the diffusion coefficient, while the pure water diffusion coefficient is a minor overestimate. In addition, GLYCAM TIP5P gives the best approximation of the quasi-linear concentration dependence observed in the experimental data.

For GLYCAM TIP3P, on the other hand, the nonlinearity of the diffusion coefficient becomes pronounced, showing an exponential decrease with increasing concentration, which is fundamentally different from the experimental data. This behavior is linked to the aggregation described above. At a very low concentration of 0.25 mol kg^{-1}, the diffusion coefficient is similar to the diffusion coefficient obtained with CHARMM TIP3P, consistent with the identical water model. The large saccharide clusters, which form at ∼0.5 mol kg^{-1}, lead to a larger bulk hydrodynamic radius and therefore a strongly reduced diffusion coefficient is observed for higher concentrations.

Although the water model clearly plays an important role, the fact that the TIP5P water model overestimates the water self-diffusion while GLYCAM TIP5P underestimates the saccharide diffusion as well as the difference in the diffusion coefficients for CHARMM TIP3P and GLYCAM TIP3P shows that, even for moderate concentrations, the water self-diffusion coefficient is not sufficient to predict the saccharide diffusion. The choice of the carbohydrate FF is a key factor for the correct system dynamics in this concentration range.

3.2. Density. The mass density of the system at different β-D-glucose concentrations is shown in Figure 4, together with the experimental values. All FFs show a logarithmic trend with increasing concentration, which is consistent with the experimental data. The best agreement with experimental values is given by the GLYCAM FF with either the TIP3P or TIP5P water model. However, with GLYCAM TIP3P errors in the local density are expected due to the aggregation. CHARMM TIP3P slightly underestimates the density at higher concentrations, while GROMOS SPC shows the largest deviation from experimental data over the entire range. A plot of the RDFs of the saccharide and the surrounding water molecules (Figure 6) reveals a larger distance of the hydration shells to the saccharide for GROMOS SPC which causes the lower density. The reason might be that GROMOS SPC is a united atom FF.

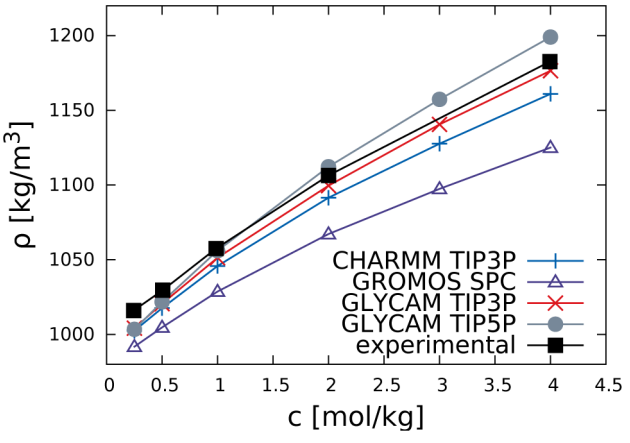

Figure 4. Mass density ρ of β-D-glucose solutions in water at different concentrations c. Results from the different FFs are shown in comparison to experimental data.[76]

3.3. Computational Efficiency. For all FFs, the simulations slow with higher β-D-glucose concentration. At a concentration of 0.25 mol kg^{-1}, GLYCAM TIP3P and CHARMM TIP3P have virtually identical computational costs. However, at a concentration of 4 mol kg^{-1}, GLYCAM TIP3P is ∼7.5% faster than CHARMM TIP3P, despite having the same number of atoms in the system, because of the more expensive Urey–Bradley potential used in the CHARMM topology, instead of the simple harmonic potential, as in GLYCAM. The average computation speed for a system of 20130 atoms with a β-D-glucose concentration of 4 mol kg^{-1} is 18.78 ns day^{-1} with GLYCAM TIP3P on two Intel Xeon X5675 CPUs using 12 cores. Switching the water model for GLYCAM from TIP3P to TIP5P decreases the computation speed by a factor of ∼2.4 at a concentration of 2 mol kg^{-1}. Unsurprisingly, as GROMOS SPC is a united atom FF, GROMOS SPC is fastest at all concentrations. The most significant advantage is observed at a concentration of 4 mol kg^{-1}, where GROMOS SPC is ∼28.5% faster than GLYCAM TIP3P.

3.4. Free Energy of Hydration: Force Field Evaluation. The results for the calculated free energies of hydration ΔG of α-D-xylose, α-D-glucose, and cellobiose are shown in Table 1, in comparison to experimental data. To our knowledge, only one study exists that reports vapor pressures for saccharides[77] using the Knudsen Effusion method. Note the large error estimate for the experimental value of cellobiose.

The range of the computed values of ΔG of the different FFs is quite large. CHARMM TIP3P and GROMOS SPC give comparable results that are significantly lower than the experimental values. Note that, for the GROMOS FF, an α-anomer can switch into a β-anomer. However, the experimental free-energy difference of this transition for D-xylose is approximately −1.59 kJ mol^{-1} (−1.37 kJ mol^{-1} for D-glucose and −1.47 kJ $mol^{-1}$for cellobiose) and therefore negligible, compared to the given experimental error.[78] Similar values for α-D-glucose have also been found in a previous study,[79] using the Generalized Amber Force Field[80] (GAFF) with TIP3P. In light of this good agreement between several FFs, the difference from the experimental value is surprisingly large, especially since GROMOS56A6$_{CARBO}$ is a modification of GROMOS53A6,[81] which was parametrized using experimental data for the free enthalpy of hydration and CHARMM has been reported to give a a reasonable agreement for the calculated free energy of hydration with experimental data for several model compounds.[47]

For GLYCAM, ΔG is strongly dependent on the water model, in contrast to the GAFF, for which the choice of the water model (TIP3P or TIP4P-Ew) was found to be of minor significance.[79] The ΔG data obtained with GLYCAM TIP3P is already closer to the experimental values than CHARMM TIP3P or GROMOS SPC; however, GLYCAM TIP5P gives

DOI: 10.1021/ct500924f
J. Chem. Theory Comput. 2015, 11, 1765−1774

Table 1. Free Energy of Hydration for α-D-Xylose, α-D-Glucose, and Cellobiose in Comparison to Experimental Data[77] at 300 K

	Free Energy of Hydration, ΔG (kJ mol^{-1})				
saccharide	experiment	GLY TIP3P	GLY TIP5P	CHARMM	GROMOS
α-D-xylose	−85.19 ± 3.12	−71.25 ± 0.09	− 87.74 ± 0.12	−57.12 ± 0.10	−57.78 ± 0.20
α-D-glucose	−104.45 ± 4.99	−90.65 ± 0.19	−110.87 ± 0.26	−66.83 ± 0.50	−72.70 ± 0.37
cellobiose	−168.7 ± 43.4	−132.40 ± 0.75	−185.55 ± 0.76	−112.97 ± 0.32	−119.75 ± 0.75

the best agreement with experimental data, with results close to the experimental error margin for α-D-glucose and well within that error for α-D-xylose and cellobiose. Note that, in all cases, GLYCAM TIP5P slightly overestimates ΔG, whereas all other FFs underestimate ΔG. Using the GLYCAM06-EP FF with TIP5P water reduces the ΔG values for α-D-glucose and cellobiose back to −90.65 kJ mol^{-1} and −134.00 kJ mol^{-1}, respectively. These values are almost identical to the ones found with GLYCAM TIP3P, suggesting that the effects of the solvent and solute lone pairs have opposite effects on the hydration.

The greater free-energy difference in GLYCAM TIP3P, compared to CHARMM TIP3P, is consistent with the stronger van der Waals interactions for carbon atoms discussed above, because they increase not only the solute−solute attraction but also the solute−solvent attraction. The free-energy differences between the FFs are very well reflected by the difference in the average potential energies shown in Table 2 for α-D-glucose.

Table 2. Average Solute−Solvent Potential Energies for α-D-Glucose at 300 K for Different FFs

	Average Solute−Solvent Potential Energy (kJ mol^{-1})		
FF	Total	LJ	Coulomb
CHARMM	−261.9 ± 0.87	−28.36 ± 0.13	−233.59 ± 0.74
GLY TIP3P	−296.0 ± 1.23	−30.6 ± 0.13	−265.38 ± 1.1
GLY TIP5P	−340.4 ± 3.28	−0.5 ± 0.18	−339.94 ± 3.1
GROMOS	−287.8 ± 0.7	−6.9 ± 0.1	−280.9 ± 0.6

The solute−solvent potential energy contribution is smallest for CHARMM TIP3P and largest for GLYCAM TIP5P. The sum of other contributions to the free-energy difference is roughly the same for all FFs, except GLYCAM TIP5P, where the large electrostatic interactions are partially compensated by a larger contribution from other factors.

The increased solute−solvent affinity for TIP5P water is due to the electrostatic interactions, whereas the contribution from the LJ interactions is much smaller than for either the TIP3P or SPC water model. Similar trends are found for cellobiose and α-D-xylose.

3.5. Free Energy of Hydration: Short Polysaccharides.

We calculate ΔG for linear polysaccharides with a DP up to 16 using the GLYCAM TIP5P FF, since it gave the best agreement with the experimental data above. The results shown in Figure 5a for β-D-glucose and the epimer β-D-mannose are almost identical, whereas ΔG for β-D-xylose, which is missing the C6 chain including an hydroxyl group, in comparison to β-D-glucose, is larger (less negative). Consistently, the values of ΔG for a mixed polysaccharide consisting of alternating β-D-glucose and β-D-xylose lies between that of a pure β-D-glucose and a pure β-D-xylose polysaccharide.

Although the plots appear linear, the free energy of hydration per monomer ΔG DP^{-1} shown in Figure 5b increases with DP for short chains. However, the increase in ΔG DP^{-1} becomes smaller for larger polysaccharides and appears to converge as the end monomers becomes less significant, so that an estimate for the free energy of hydration of longer linear polysaccharides can be obtained. Each monomer has equatorially positioned hydroxyl groups that can form hydrogen bonds either with the molecule itself or with the water molecules. Each glycosidic bond uses one of the hydroxyl groups from each monomer, so that central monomers in a polymer have fewer possibilities of forming hydrogen bonds than terminal or single monomers. Although not entirely constant, values of ΔG per hydroxyl group converges quickly to values between −21.5 kJ/mol and −22.5 kJ/mol for β-D-glucose and β-D-xylose. Surprisingly, despite its structural similarity to β-D-glucose, for β-D-mannose, the hydration free energy per hydroxyl group is significantly lower (−23.5 kJ/mol). In the next section, we further investigate the interactions of the saccharides with water, which lead to this relationship.

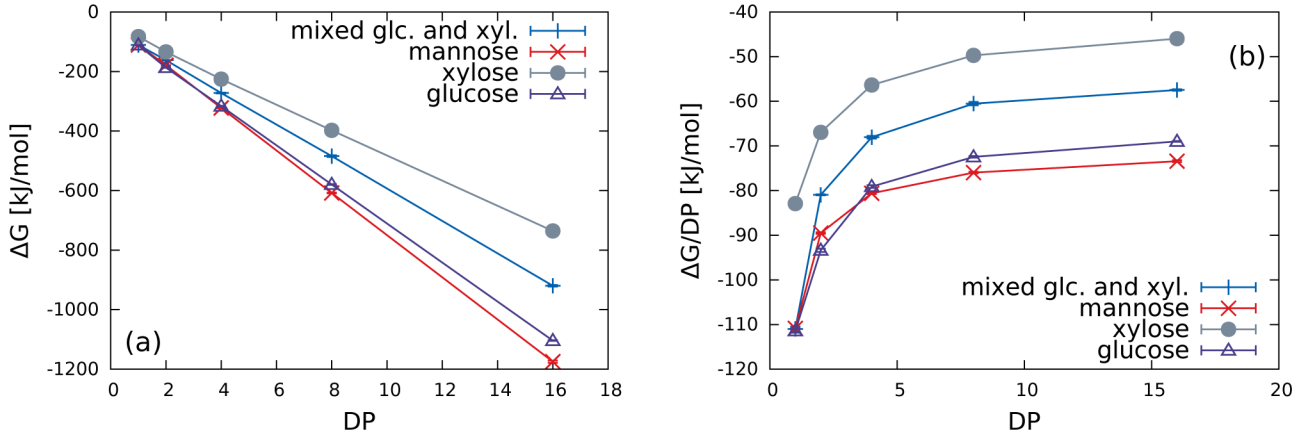

Figure 5. Free energy of hydration ΔG for different polysaccharides as a function of DP. ΔG is plotted (a) for the entire polysaccharide and (b) per monomer. Note that the error bars are smaller than the symbols.

DOI: 10.1021/ct500924f
J. Chem. Theory Comput. 2015, 11, 1765−1774

3.6. Polysaccharide Hydration Characteristics. First, we look at the RDF of water molecules (COM) around a monomer (COM) inside a polysaccharide with DP = 1−16 for the GLYCAM TIP5P FF. For better comparability, a central monomer of the polysaccharide is chosen. The RDFs of monomers that are not in the center of the polysaccharide show only minor differences to the respective position in a smaller polysaccharide; for example, an end monomer in a tetramer is comparable to a monomer in a dimer with minor deviations. Note that, for monomers and dimers, we exclude the atoms O1, HO1, and HO4 (see Figure 1a) from the RDF calculation for better comparability. The results for polysaccharides consisting only of β-D-glucose monomers, plotted in Figure 6, show that

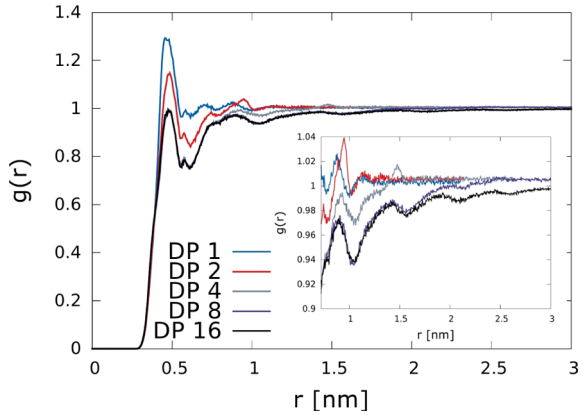

Figure 6. RDFs of water molecules (COM) around the COM of a central monomer inside a β-D-glucose polysaccharide with different DP values. The inset shows a larger view of the fine differences at greater DP values.

the notable reduction in ΔG DP^{-1}, up to DP = 4, reflects the reduction of the number of water molecules around the monomers. For DP >4, the effect becomes less significant.

Figure 7 shows the hydration number per monomer n for the different polysaccharides explicitly. Here, no atoms were

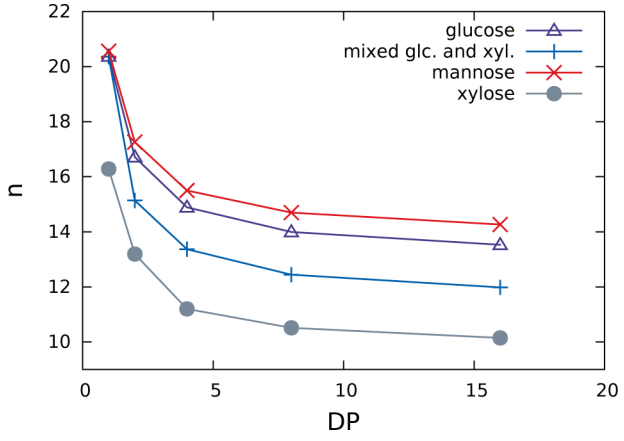

Figure 7. Hydration number per monomer n for different polysaccharides, as a function of DP.

excluded and the calculation was not restricted to central monomers. Again, the greatest change is observed for small DPs up to four, but here small differences at a higher DP become more visible and show a pattern that is roughly reflection symmetric to ΔG DP^{-1} in Figure 5b for each set of polysaccharides.

A related property is the distribution of hydrogen bonds in the system. The number of solute−solvent hydrogen bonds per monomer n_W, shown in Figure 8a, reveals a similar pattern as the hydration number in Figure 7. It decreases with higher DP, appears to converge for all polysaccharides and is consistent with ΔG DP^{-1}.

The plots show that, whereas the configurational difference between β-D-glucose and β-D-mannose allows fewer water molecules in the vicinity of the monomers, consistent with the slightly lower ΔG results, this does not appear to affect the capability for β-D-mannose, in comparison to β-D-glucose, to form solute−solvent hydrogen bonds.

On the other hand, the average number of intramolecular hydrogen bonds per monomer n_I, plotted in Figure 8b, is much lower in β-D-mannose than in β-D-glucose. However, a comparison of n_I and n_W shows that solute−solvent hydrogen bonds occur far more frequently than intramolecular hydrogen bonds, so that the competition between intramolecular and solute−solvent hydrogen bonding is significant only for molecular conformations, but should have little effect on the solute−solvent interactions.

Nonetheless, the patterns in Figure 8b reflect some features of the chemical structure worth investigating. In the following analysis, we consider only hydrogen bonds with an occupancy of ≥0.5% to be significant. The number of intramolecular hydrogen bonds per monomer in β-D-glucose and β-D-mannose polysaccharides increases with DP. Unlike n_W, the number of intramolecular hydrogen bonds differ strongly between β-D-glucose and β-D-mannose polysaccharides. The most frequent intramolecular hydrogen bond in β-D-glucose polysaccharides, with an occupancy of 8.7% for dimers, is HO3···O5 between adjacent bonded monomers shown in Figure 9a. This hydrogen bond stabilizes the main conformation of the glycosidic dihedral angles. The other possibility for intramolecular hydrogen bond formation, with a significantly lower occupancy of 0.5% for dimers, is HO6···O2 (also shown in Figure 9a). In β-D-mannose polysaccharides, the different configuration of the second hydroxyl group prevents the HO6···O2 hydrogen bond. Therefore, for β-D-mannose polysaccharides, the only significant hydrogen bond is HO3···O5 with an occupancy of 4.0% for dimers, which also occurs in the β-D-glucose polysaccharides.

In β-D-xylose, which is missing the C6 chain, the fourth hydroxyl group can flip over as the electrostatic interactions stabilizing its position in β-D-glucose and β-D-mannose are absent. Therefore, β-D-xylose can form the intramonomer hydrogen bond HO4···O2 shown in Figure 9b. Note that, in this case, we have a $^1C_4$ chair conformation and not the most prevalent $^4C_1$ chair conformation. The $^1C_4$ chair conformation can also be observed using the other FFs. In the dimer, the intramonomer hydrogen bonds are HO4···O2 as well as HO2···O4. The HO3···O5 hydrogen bond is found with a significantly lower occupancy of 1.2% for dimers, in comparison to 8.7% for β-D-glucose dimers.

For the β-D-xylose, polysaccharides, the HO4···O2 intramonomer hydrogen bond is only significant for the first monomer in the polymer since, for all other monomers, the O4 is occupied by the covalent bond linking the monomers, and thus prevents hydrogen bonding for neighboring monomers. The decreasing importance of the HO4···O2 bond with

DOI: 10.1021/ct500924f
J. Chem. Theory Comput. 2015, 11, 1765−1774

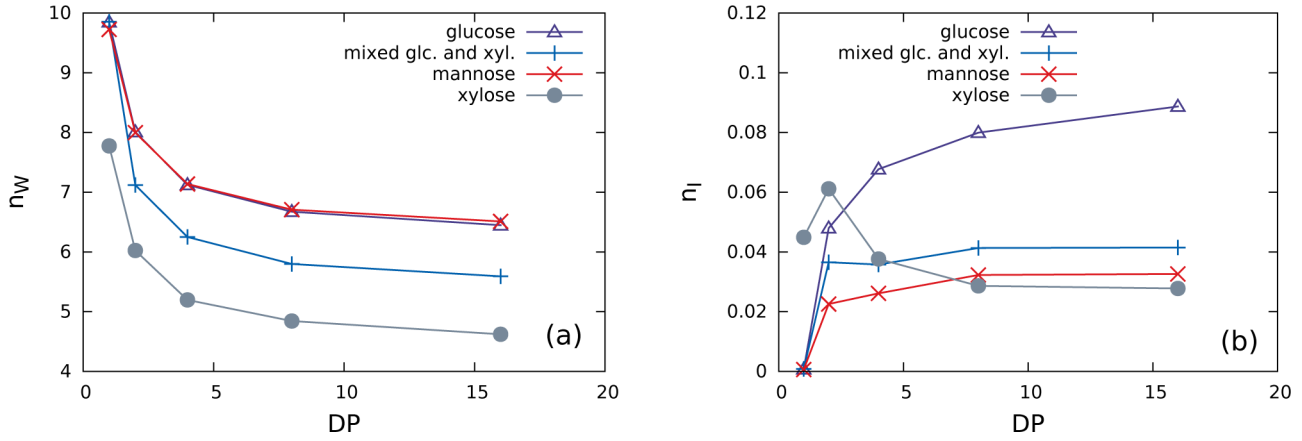

Figure 8. Average number of hydrogen bonds per monomer for different polysaccharides as a function of DP: (a) the number of solute−solvent hydrogen bonds n_W and (b) the number of intramolecular hydrogen bonds n_I.

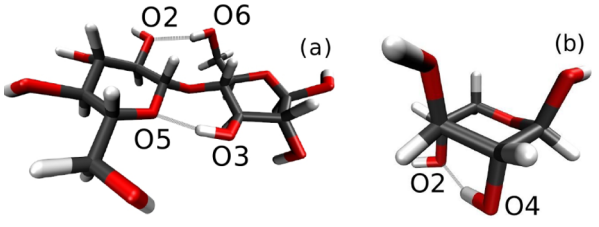

Figure 9. (a) Cellobiose with HO3···O5 and HO6···O2 hydrogen bonds. (b) β-D-Xylose with HO4···O2 hydrogen bond.

increasing DP leads to the initial increase and following decrease of n_I with higher DP seen in Figure 8b.

In the mixed β-D-glucose and β-D-xylose polysaccharide, the monomer (DP = 1) is β-D-glucose, so there are no intramolecular hydrogen bonds. For DP > 1, the main hydrogen bond is HO3···O5; however, in comparison to pure β-D-glucose polysaccharides, the hydrogen bond HO3···O5 has a significantly lower occupancy of 2.1% for dimers in the mixed saccharide. In addition, we have a hydrogen bond $HO3_{xyl}$···$O6_{glc}$ with an occupancy of 0.5% for dimers, which can be formed only every second bond and is competing with the HO3···O5 hydrogen bond. For all other polymers, this hydrogen bond has an occupancy below 0.2% explaining the peak for the dimer.

Except for the polysaccharides built of β-D-glucose, n_I appears to have converged to a constant for DP = 8.

4. CONCLUSIONS

We have compared four common polysaccharide FFs, with respect to their solution properties and molecular interactions with water. All FFs except GLYCAM TIP3P show the correct trends for the aggregation and diffusion properties at moderate concentrations. For GLYCAM TIP3P, aggregation sets in at nonphysically low concentrations of 0.5 mol kg^{-1}, limiting its application to single molecules or very low concentration systems. Inversely, no FF except GLYCAM TIP3P shows aggregation, even well above the solubility limit.

Overall, GLYCAM TIP5P was found to give the best quantitative agreement with experimental data for diffusion, system density, and the free energy of hydration. Based on these results, we conclude that GLYCAM TIP5P is best suited for studying oligosaccharides, such as the plant cell wall saccharides in solution. If computational efficiency is the limiting factor, $GROMOS56A6_{CARBO}$ SPC is an alternative that provides similar structural features, but with the limitations described above and limited parametrized monomers.

Application of the GLYCAM TIP5P FF to short plant cell wall polysaccharides shows that the difference in the free energy of hydration for different constituting monomers is mainly determined by the number of free hydroxyl groups. The values of the free energy of hydration are consistent with the hydration number, the number of hydrogen bonds with water, and the RDFs of water molecules around the monomers, whereas the ability to form intramolecular hydrogen bonds has a negligible effect for the short polysaccharides investigated here.

AUTHOR INFORMATION

Corresponding Author

*E-mail: andrea.grafmueller@mpikg.mpg.de.

Notes

The authors declare no competing financial interest.

ACKNOWLEDGMENTS

The project was funded by the Deutsche Forschungsgemeinschaft (No. GR 3661/2-1). The authors thank Reinhard Lipowsky and Robert J. Woods for helpful discussions.

REFERENCES

(1) Pauly, M.; Keegstra, K. *Plant J.* **2008**, *54*, 559−568.
(2) Fratzl, P.; Gupta, H.; Burgert, I. *Comp. Biochem. Physiol., Part A: Mol. Integr. Physiol.* **2007**, *146*, S132−S132.
(3) Yamamoto, H.; Ruelle, J.; Arakawa, Y.; Yoshida, M.; Clair, B.; Gril, J. *Wood Sci. Technol.* **2010**, *44*, 149−163.
(4) Schreiber, N.; Gierlinger, N.; Puetz, N.; Fratzl, P.; Neinhuis, C.; Burgert, I. *Plant J.* **2010**, *61*, 854−861.
(5) Burgert, I.; Eder, M.; Gierlinger, N.; Fratzl, P. *Planta* **2007**, *226*, 981−987.
(6) Harrington, M. J.; Razghandi, K.; Ditsch, F.; Guiducci, L.; Rueggeberg, M.; Dunlop, J. W. C.; Fratzl, P.; Neinhuis, C.; Burgert, I. *Nat. Commun.* **2011**, *2*, 337.
(7) Dawson, C.; Vincent, J. F. V.; Rocca, A.-M. *Nature* **1997**, *390*, 668−668.
(8) Scheller, H. V.; Ulvskov, P. *Plant Biol.* **2010**, *61*, 263.
(9) Fry, S. C. *J. Exp. Bot.* **1989**, *40*, 1−11.
(10) Wyman, C. E.; Decker, S. R.; Himmel, M. E.; Brady, J. W.; Skopec, C. E.; Viikari, L. In *Polysaccharides: Structural Diversity and Functional Versatility*; CRC Press: New York, 2005; pp 995−1035.

DOI: 10.1021/ct500924f
J. Chem. Theory Comput. 2015, 11, 1765−1774

(11) Vincken, J.-P.; York, W. S.; Beldman, G.; Voragen, A. *Plant Physiol.* **1997**, *114*, 9.
(12) Beckham, G. T.; Bomble, Y. J.; Bayer, E. A.; Himmel, M. E.; Crowley, M. F. *Curr. Opin. Biotechnol.* **2011**, *22*, 231−238.
(13) Bellesia, G.; Asztalos, A.; Shen, T.; Langan, P.; Redondo, A.; Gnanakaran, S. *Acta Crystallogr., Sect. D: Biol. Crystallogr.* **2011**, *66*, 1184−1188.
(14) Yamane, C.; Miyamoto, H.; Hayakawa, D.; Ueda, K. *Carbohydr. Res.* **2013**, *379*, 30−37.
(15) Beckham, G. T.; Matthews, J. F.; Peters, B.; Bomble, Y. J.; Himmel, M. E.; Crowley, M. F. *J. Phys. Chem. B* **2011**, *115*, 4118−4127.
(16) Payne, C. M.; Himmel, M. E.; Crowley, M. F.; Beckham, G. T. *J. Phys. Chem. Lett.* **2011**, *2*, 1546−1550.
(17) Bergenstrahle, M.; Wohlert, J.; Himmel, M. E.; Brady, J. W. *Carbohydr. Res.* **2010**, *345*, 2060−2066.
(18) Payne, C. M.; Himmel, M. E.; Crowley, M. F.; Beckham, G. T. *J. Phys. Chem. Lett.* **2011**, *2*, 1546−1550.
(19) Zhao, Y.; Liu, X.; Wang, J.; Zhang, S. *Carbohydr. Polym.* **2013**, *94*, 723−730.
(20) Payal, R. S.; Balasubramanian, S. *Phys. Chem. Chem. Phys.* **2014**, *16*, 17458−17465.
(21) Matthews, J. F.; Bergenstrahle, M.; Beckham, G. T.; Himmel, M. E.; Nimlos, M. R.; Brady, J. W.; Crowley, M. F. *J. Phys. Chem. B* **2011**, *115*, 2155−2166.
(22) Bergenstråhle, M.; Berglund, L. A.; Mazeau, K. *J. Phys. Chem. B* **2007**, *111*, 9138−9145.
(23) Umemura, M.; Yuguchi, Y. *Carbohydr. Res.* **2005**, *340*, 2520−2532.
(24) Hanus, J.; Mazeau, K. *Biopolymers* **2006**, *82*, 59−73.
(25) Zhang, Q.; Brumer, H.; Ågren, H.; Tu, Y. *Carbohydr. Res.* **2011**, *346*, 2595−2602.
(26) Zhao, Z.; Crespi, V. H.; Kubicki, J. D.; Cosgrove, D. J.; Zhong, L. *Cellulose* **2014**, *21*, 1025−1039.
(27) Mazeau, K.; Charlier, L. *Cellulose* **2012**, *19*, 337−349.
(28) Umemura, M.; Yuguchi, Y. *Cellulose* **2009**, *16*, 361−371.
(29) Fadda, E.; Woods, R. J. *Drug Discovery Today* **2010**, *15*, 596−609.
(30) Foley, B. L.; Tessier, M. B.; Woods, R. J. *WIREs Comput. Mol. Sci.* **2012**, *2*, 652−697.
(31) Matthews, J. F.; Beckham, G. T.; Bergenstrahle-Wohlert, M.; Brady, J. W.; Himmel, M. E.; Crowley, M. F. *J. Chem. Theory Comput.* **2012**, *8*, 735−748.
(32) Nicholls, A.; Mobley, D. L.; Guthrie, J. P.; Chodera, J. D.; Bayly, C. I.; Cooper, M. D.; Pande, V. S. *J. Med. Chem.* **2008**, *51*, 769−779.
(33) Mobley, D. L.; Bayly, C. I.; Cooper, M. D.; Shirts, M. R.; Dill, K. A. *J. Chem. Theory Comput.* **2009**, *5*, 350−358.
(34) Mobley, D. L.; Dumont, É; Chodera, J. D.; Dill, K. A. *J. Phys. Chem. B* **2007**, *111*, 2242−2254.
(35) Mobley, D. L.; Bayly, C. I.; Cooper, M. D.; Dill, K. A. *J. Phys. Chem. B* **2009**, *113*, 4533−4537.
(36) Geballe, M. T.; Skillman, A. G.; Nicholls, A.; Guthrie, J. P.; Taylor, P. J. *J. Comput.-Aided Mol. Des.* **2010**, *24*, 259−279.
(37) Pronk, S.; Páll, S.; Schulz, R.; Larsson, P.; Bjelkmar, P.; Apostolov, R.; Shirts, M. R.; Smith, J. C.; Kasson, P. M.; van der Spoel, D. *Bioinformatics* **2013**, *29*, 845−854.
(38) Hess, B.; Bekker, H.; Berendsen, H. J.; Fraaije, J. G. *J. Comput. Chem.* **1997**, *18*, 1463−1472.
(39) Miyamoto, S.; Kollman, P. A. *J. Comput. Chem.* **1992**, *13*, 952−962.
(40) Darden, T.; York, D.; Pedersen, L. *J. Chem. Phys.* **1993**, *98*, 10089−10092.
(41) Parrinello, M.; Rahman, A. *J. Appl. Phys.* **1981**, *52*, 7182−7190.
(42) Nose, S.; Klein, M. *Mol. Phys.* **1983**, *50*, 1055−1076.
(43) Birdsall, C. K., Langdon, A. B. *Plasma Physics via Computer Simulation*; McGraw−Hill: New York, 1985.
(44) Nosé, S. *J. Chem. Phys.* **1984**, *81*, 511−519.
(45) Hoover, W. G. *Phys. Rev. A* **1985**, *31*, 1695.
(46) Van Gunsteren, W.; Berendsen, H. *Mol. Simul.* **1988**, *1*, 173−185.
(47) Guvench, O.; Greene, S. N.; Kamath, G.; Brady, J. W.; Venable, R. M.; Pastor, R. W.; Mackerell, A. D. *J. Comput. Chem.* **2008**, *29*, 2543−2564.
(48) Guvench, O.; Hatcher, E.; Venable, R. M.; Pastor, R. W.; MacKerell, A. D., Jr. *J. Chem. Theory Comput.* **2009**, *5*, 2353−2370.
(49) Hansen, H. S.; Hünenberger, P. H. *J. Comput. Chem.* **2011**, *32*, 998−1032.
(50) Jorgensen, W. L.; Chandrasekhar, J.; Madura, J. D.; Impey, R. W.; Klein, M. L. *J. Chem. Phys.* **1983**, *79*, 926−935.
(51) Berendsen, H. J., Postma, J., van Gunsteren, W., Hermans, J. *Intermolecular Forces*; Springer: New York, 1981; pp 331−342.
(52) Kirschner, K. N.; Yongye, A. B.; Tschampel, S. M.; González-Outeirino, J.; Daniels, C. R.; Foley, B. L.; Woods, R. J. *J. Comput. Chem.* **2008**, *29*, 622−655.
(53) Case, D. A.; Darden, T. A.; Cheatham, T. E., III; Simmerling, C. L.; Wang, J.; Duke, R. E.; Luo, R.; Walker, R.; Zhang, W.; Merz, K.; Kollman, P. A. *AMBER 12*; University of California, San Francisco, 2012.
(54) Woods Group . (2005-2015) *GLYCAM Web*; Complex Carbohydrate Research Center, University of Georgia: Athens, GA; available via the Internet at http://www.glycam.com.
(55) Sorin, E. J.; Pande, V. S. *Biophys. J.* **2005**, *88*, 2472−2493.
(56) Wehle, M.; Vilotijevic, I.; Lipowsky, R.; Seeberger, P. H.; Varon Silva, D.; Santer, M. *J. Am. Chem. Soc.* **2012**, *134*, 18964−18972.
(57) Mahoney, M. W.; Jorgensen, W. L. *J. Chem. Phys.* **2000**, *112*, 8910−8922.
(58) Humphrey, W.; Dalke, A.; Schulten, K. *J. Mol. Graph.* **1996**, *14*, 33−38.
(59) Einstein, A. *Ann. Phys.* **1905**, *322*, 549−560.
(60) Bennett, C. H. *J. Comput. Phys.* **1976**, *22*, 245−268.
(61) Shirts, M. R., Mobley, D. L. *Biomolecular Simulations*; Springer: New York, 2013; pp 271−311.
(62) Shirts, M. R.; Pande, V. S. *J. Chem. Phys.* **2005**, *122*, 144107.
(63) de Ruiter, A.; Boresch, S.; Oostenbrink, C. *J. Comput. Chem.* **2013**, *34*, 1024−1034.
(64) Wu, D.; Kofke, D. A. *J. Chem. Phys.* **2005**, *123*, 054103.
(65) Beutler, T. C.; Mark, A. E.; van Schaik, R. C.; Gerber, P. R.; van Gunsteren, W. F. *Chem. Phys. Lett.* **1994**, *222*, 529−539.
(66) van der Spoel, D.; Lindahl, E.; Hess, B. and The GROMACS Development Team; *GROMACS User Manual* version 4.6.5., 2013; www.gromacs.org.
(67) *Sigma−Aldrich Product Information*; available via the Internet at: http://www.sigmaaldrich.com/content/dam/sigma-aldrich/docs/Sigma/ProductInformationSheet/2/g8270pis.pdf.
(68) Hadden, J. A.; French, A. D.; Woods, R. J. *Biopolymers* **2013**, *99*, 746−756.
(69) Tschampel, S. M.; Kennerty, M. R.; Woods, R. J. *J. Chem. Theory Comput.* **2007**, *3*, 1721−1733.
(70) Limbach, H. J.; Ubbink, J. *Soft Matter* **2008**, *4*, 1887−1898.
(71) Molinero, V.; Goddard, W. A., III. *Phys. Rev. Lett.* **2005**, *95*, 045701.
(72) Gladden, J.; Dole, M. *J. Am. Chem. Soc.* **1953**, *75*, 3900−3904.
(73) Venable, R. M.; Hatcher, E.; Guvench, O.; MacKerell, A. D., Jr; Pastor, R. W. *J. Phys. Chem. B* **2010**, *114*, 12501−12507.
(74) Mahoney, M. W.; Jorgensen, W. L. *J. Chem. Phys.* **2001**, *114*, 363−366.
(75) Holz, M.; Heil, S. R.; Sacco, A. *Phys. Chem. Chem. Phys.* **2000**, *2*, 4740−4742.
(76) Taylor, J.; Rowlinson, J. *Trans. Faraday Soc.* **1955**, *51*, 1183−1192.
(77) Oja, V.; Suuberg, E. *J. Chem. Eng. Data* **1999**, *44*, 26−29.
(78) Kabayama, M.; Patterson, D.; Piche, L. *Can. J. Chem.* **1958**, *36*, 557−562.
(79) Klimovich, P. V.; Mobley, D. L. *J. Comput.-Aided Mol. Des.* **2010**, *24*, 307−316.
(80) Wang, J.; Wolf, R. M.; Caldwell, J. W.; Kollman, P. A.; Case, D. A. *J. Comput. Chem.* **2004**, *25*, 1157−1174.

DOI: 10.1021/ct500924f
J. Chem. Theory Comput. 2015, 11, 1765−1774

(81) Oostenbrink, C.; Villa, A.; Mark, A. E.; Van Gunsteren, W. F. *J. Comput. Chem.* **2004**, *25*, 1656−1676.

DOI: 10.1021/ct500924f
J. Chem. Theory Comput. 2015, 11, 1765−1774